
Article:
Yildirimli, K. orcid.org/0000-0001-7739-8342, Boschetti Pereira, H., Goldenstein, H. et al. (3 more authors) (2024) Scaling-up laser cladding of rails. Wear, 540-541. 205227. ISSN 0043-1648

https://doi.org/10.1016/j.wear.2023.205227

Wear 540-541 (2024) 205227

Contents lists available at ScienceDirect

Wear

journal homepage: www.elsevier.com/locate/wear

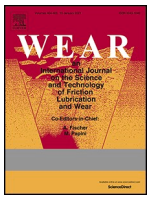

Scaling-up laser cladding of rails

K. Yildirimli [a,*], H. Boschetti Pereira [b], H. Goldenstein [b], D.I. Fletcher [a], Z.S. Lee [a], R. Lewis [a]

[a] The University of Sheffield, Department of Mechanical Engineering, Sheffield, UK
[b] Universidade de São Paulo, Metallurgical and Materials Engineering Department, São Paulo, Brazil

ARTICLE INFO

Keywords:
Laser cladding
Rail steel
Wear reduction
Twin-disc testing
Full-scale testing

ABSTRACT

With rail travel getting more popular more demands are being put on rail infrastructure. The wheel/rail contact is the one of the main parameters that is key to maintaining a high performing network. With increasing demands for higher loads and higher speeds, wear and rolling contact fatigue (RCF) are the main two problems.

New maintenance techniques can overcome some problems, but new solutions that reduce the damage are needed. Laser cladding is one of the best methods for improving wear and RCF of rail steels by adding layers of more durable materials to the rail.

In this article full-scale tests of clad layers have been carried out at realistic contact conditions to verify outcomes seen in twin-disc testing to see if the results can be scaled to predict field performance of clad layers. Martensitic Stainless Steel (MSS) and Stellite 6 were used for the clad layers and R260 was used as the base material. Un-clad R260 was used as reference material.

Results of full-scale tests in terms of wear rates, sub-surface deformation, hardness and roughness evolution were comparable. This showed that the clad layers deposited on actual rail performed very well compared to un-clad rail and that the tests run at the small-scale were appropriate for predicting full-scale behaviour.

1. Introduction

Rail travel is getting more popular day by day. The rail network in the UK is ordinarily extremely busy as it is shared by freight and passenger trains. The increasing population of the passengers who are using rail travel is leading to more trains with greater loads and increasing train speeds which is leading to more severe wheel/rail contact. This can cause more wear and possibly rolling contact fatigue (RCF). Wear and RCF can cause rail failures and the need for rail replacement or repair across different railway track components such as plain line, insulated block joints (IBJ) or switches and crossings [1]. RCF can be seen in various forms such as: shelling, head checks, corner-gauge crack and flaking, these defects are caused by initiation of cracks and their propagation in the rail material. Left untreated these surface-initiated cracks could cause failure of rail and even derailment [2,3].

Maintenance is expensive and must be planned carefully to minimise disruption to the network as engineering work requires track closure, reducing capacity. Extending the life of the rail can help sustainability and reduce the costs associated with rail replacement. New materials are being developed and new processing techniques are being used to increase the lifespan of rail. Surface treatments including case hardening, peening and surface coatings can be used to improve wear and RCF performance of rail materials.

The deposition of a surface layer of premium material with benefits such as wear and rolling contact fatigue resistance, higher yield strength and less susceptibility to plastic deformation is a desirable method to increase the durability of rail whilst retaining the cost and strength advantages of bulk rail steels. Additive manufacturing with laser clad coatings can be used for adding premium materials to a standard grade substrate material. Laser cladding can enhance rail durability; the process can be used with a choice of rail materials dependent on required properties or position in track providing beneficial opportunities for rail improvements [4,5].

In the cladding process (illustrated in Fig. 1), while a cladding material is added to the surface of the substrate, a high energy laser is passed over that surface. The laser melts the surface of the substrate material and the coating material successively and welds them together. When the laser beam creates a melt pool, powder is injected into the pool and the particles melt and a single track of the clad is created. This process can be repeated for a second layer over the first layer of clad material so large thicknesses can be built-up if required [3,4,6,8].

Prior to field testing, a series of small-scale tests were required to

* Corresponding author.
E-mail address: kyildirimli1@sheffield.ac.uk (K. Yildirimli).

https://doi.org/10.1016/j.wear.2023.205227
Received 27 February 2023; Received in revised form 21 September 2023; Accepted 26 December 2023
Available online 30 December 2023

complete the understanding of the process capabilities and answer safety questions. Research in small scale, additive manufacturing with laser clad coatings has previously shown promising results in laboratory tests for reducing wear in rail and extending rail life. Laser clad rail specimen tests showed improved properties than normal grade rail specimens on small-scale twin disc tests. Bending tests were conducted in previous research for MSS clad on a R260 rail substrate. After the four-point bending tests, it was found that MSS clad over R260 rail did not fail within 5,000,000 cycles in tested carried out with a 350 MPa stress range which is much higher than the standard requirements for fatigue strength of about 230 MPa [10]. Martensitic Stainless Steel (MSS) clad and Stellite 6 clad in particular have been shown to have a lower wear rate and higher RCF resistance than R260 standard grade rail specimens [9]. In another study of MSS clad rail discs and unclad R260 rail discs in small-scale laboratory tests it was shown that cladding onto a lower grade rail (in this case R200) the same benefits in terms of wear and RCF resistance were achieved [10]. Furthermore, other RCF tests showed R260 grade rails failing around 15,000 small scale twin disc cycles, whereas Stellite 6 clad rail disc did not show any failure signs at over 50,000 cycles [4]. In fact, this was subsequently shown to still be the case after 400,000 cycles [11].

There are more small-scale tests that have shown improved wear and RCF performance on clad rail discs. Research has mainly been focused on cladding new rail, but repair has been considered [1,11–13]. Mostly researchers have investigated the application of harder materials. Only one study has used a like-on-like material approach, which shows much greater benefits [13]. Alongside testing commercial materials, new microstructures have emerged in small scale testing [14,15]. Tools have been also developed for layer design, for example, for determining layer thickness [16] and plasticity [17].

There are only a few studies on full-scale tests for laser clad rail performance. Laser cladding of the rail still needs more actual wheel and rail tests to simulate real operating conditions using the full-scale component geometries in laboratory and field tests to give the railway industry confidence that the process is viable. Some initial work has been carried out looking at material flow at Insulated Block Joints [1] and field testing of clad layers to protect the heat affected zones around welded joints [18], but more is needed on wear properties.

The aim of this work was to carry out full-scale wear tests on clad layers applied to R260 rail material. MSS and Stellite 6 clad materials were chosen due to their high performance in small-scale wear and RCF resistance. The intention was to see if the same high performance could be achieved as it was in small-scale tests as the move is made towards field implementation.

2. Experimental details

2.1. Full-scale machine

Fig. 2(a) shows a schematic diagram of the linear full-scale test machine used for the tests. For a cycle of a test, first vertical force is applied to load the wheel on the rail, then the rail is pulled under the loaded wheel using one horizontal actuator. At the same time, another actuator attached to a chain mounted on the wheel, pulls this so that slip in the contact can be achieved. That vertical load of the wheel can go to a maximum limit of 200 kN while the horizontal actuators have a limit of 60 kN [1,19,20].

2.2. Specimens

Pocket specimens were chosen to test the clad layers and R260 reference material rather than cladding long lengths of rail material (see Fig. 2(b)). This meant it was easier to take measurements and analyse the specimens before and after testing. R260 is widely used rail in the UK so was the perfect choice for control and substrate for the clad layers. The chosen clad materials were MSS and Stellite 6 due to their higher performance in small-scale tribological tests and bend tests over other candidate materials [1,10].

Examined sections of the pocket specimens (see Fig. 3(a)) can be seen in Fig. 3(b)-i and Fig. 3(b)-ii showing the MSS and Stellite 6 clad layers

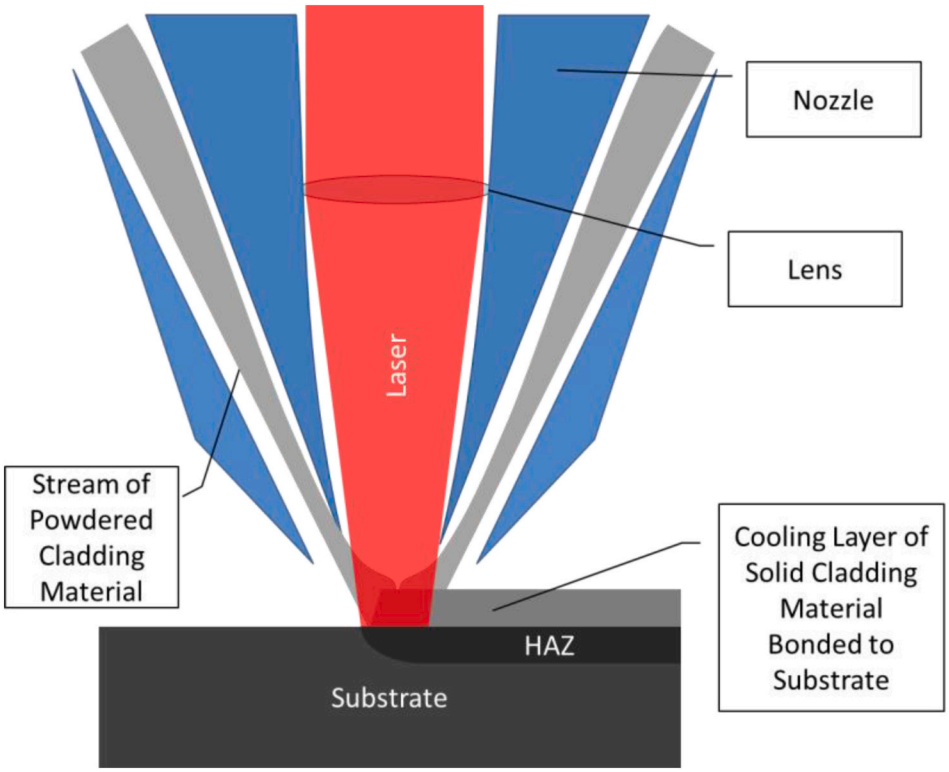

Fig. 1. Powder injection laser cladding [4].

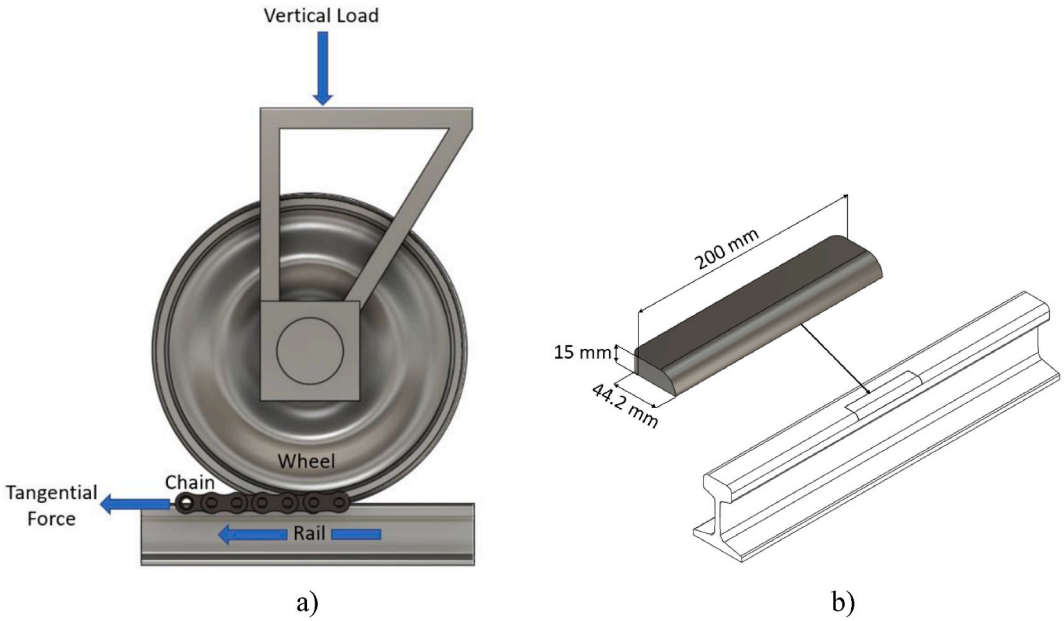

Fig. 2. Full-Scale test machine set-up: a) Schematic diagram of the full-scale wheel/rail contact rig; b) Pocket specimen inserting in the rail.

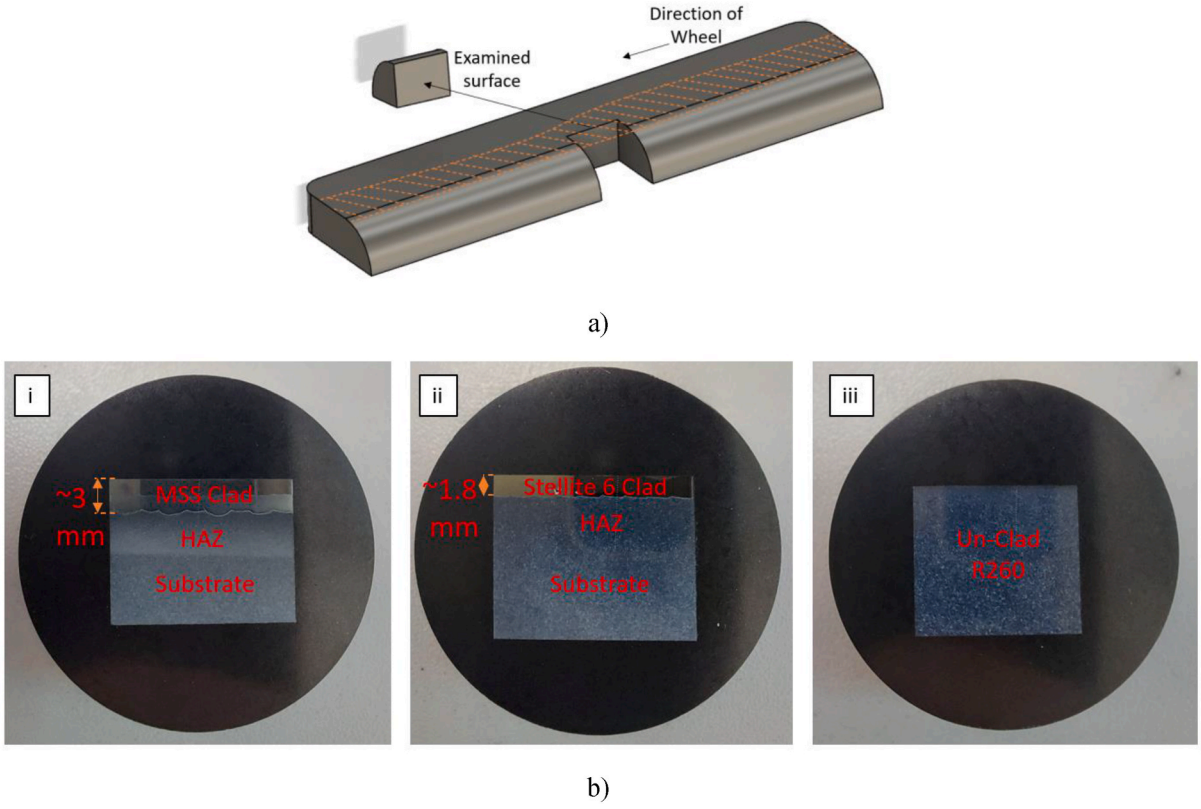

Fig. 3. Pocket specimen sectioned parts: a) Examined surface of contact path; b) Clad layer dimensions and materials.

with 3 mm and 1.8 mm respectively. This difference was not planned but resulted from something that occurred during the pre-machining/cladding/post-cladding machining process. The peak shear stress sub-surface for both specimens was within the clad layer so the difference thickness was not thought to have any effect on the differences seen in performance. After the cladding process, pocket specimens were ground to achieve that layer thicknesses. The etched part of the substrate shows the HAZ clearly. The un-clad R260 rail pocket specimen section can be seen in Fig. 3(b)-ii.

The wheel is made from R7 steel and had a roughness of 1.4 μm, Sa.

2.3. Test method and specimen analysis

The pocket specimens were cleaned with acetone and weighed, then their profiles scanned (as described below) before the start of the test and recorded. After that pocket specimen inserted into the rail and then

the pocket specimen surfaces were cleaned with acetone and left until dry. Then dry cycles were run until measurable wear was achieved on pocket specimen which occurred at 5000 cycles. After the 5000 cycles, the test rig was stopped, and wear debris of the pocket specimens were collected and then pocket specimens were taken out from the rail for examination.

The pocket specimens were cleaned with acetone and immediately weighed again. Laboratory temperature and humidity were recorded before and after the test. The rail surfaces were examined using an optical (non-contact) Alicona Infinite-Focus SL profilometer before and after the test. The profilometer provides high-resolution images and 3D surface profiles measurements with a vertical resolution of up to 10 nm. Surface roughness' were determined from the Alicona scans.

After that, pocket specimen profiles were measured using a Calipri profilometer and a Creaform HandyScan 3D laser scanner. Then pocket specimens were sectioned (Buehler Abrasimet 250), mounted (Simplimet 1000), ground and polished (Buehler Automet 250 Pro). The specimens were etched for microstructure analysis. All specimens were etched first with %2 Nital etchant to examine the R260 substrate and HAZ regions as well as the Stellite 6 clad layer. The MSS clad layer was etched with Vilella to highlight its microstructure. Viella's reagent was prepared with 1 g picric acid, 5 ml HCl and 100 ml IMS mixture [17]. Micro-hardness measurements (DuraScan) were taken on the sectioned specimens from the surface into the bulk material and nano-hardness measurements were taken near the surface (Bruker Hysitron TS77 Select).

To allow comparison between full-scale rig tests and the previous data obtained through small-scale twin disc testing the contact conditions had to be similar to those used in that work. As such, the contact stress used was 1500 MPa (by applying 110 kN) as it is the most common pressure used in small scale twin disc tests. Also, the slip ratio used was 1 %. The conditions used have been chosen to represent those typical of the rail head, wheel tread region of the wheel/rail interface for the UK passenger train network (see Ref. [31] for typical value ranges). This is the region that is being considered currently for laser cladding rather that the gauge corner in curves where more severe conditions are present.

3. Results

3.1. Surface morphology

Fig. 4 shows the pocket specimen images after the 5000 cycles of full-scale tests. Wear bands can be clearly seen in the images. The R260 pocket sample has widest and most significant wear band. Those on the MSS and Stellite 6 clad layers are very similar.

Fig. 5 shows the pocket specimen profiles before and after the completed tests. The most obviously changed profile after the tests is that on the un-clad R260 pocket specimen. Material flow/plastic deformation of the contact surface can be seen. MSS Clad and Stellite 6 clad pocket specimens do not show any evidence of plastic flow, which is not unexpected given their high hardness.

Laser scans were used after the completed tests on the pocket specimens which allowed both 2D and 3D comparisons (see Fig. 6). Scanned clad pocket specimens were compared with the un-clad reference pocket and each other. The reference pocket specimen 2D profile is seen on the left hand images as white coloured lines and the other pocket specimens are shown as a lines with a colour gradient. For the 3D scans the reference is grey. The colours refer to the height difference in mm on the images from the reference pocket specimen. The scale was chosen from 0.200 mm to −0.200 mm to show profile differences for the 3D pocket specimen scans. The 2D profiles were taken from sections in the centre of the 3D scan as shown using software in the Creaform 3D laser scanner.

The MSS-Stellite 6 pocket specimen comparison can be seen as showing the lowest difference between the two profiles. In this comparison, MSS was chosen as the reference and shown with a white line and Stellite 6 can be seen with the coloured line which is lower than the MSS pocket profile (indicating that the Stellite 6 wore more). The MSS-R260 pocket profile comparison can be seen in the middle image of Fig. 6. The MSS pocket specimens were chosen as the reference for the

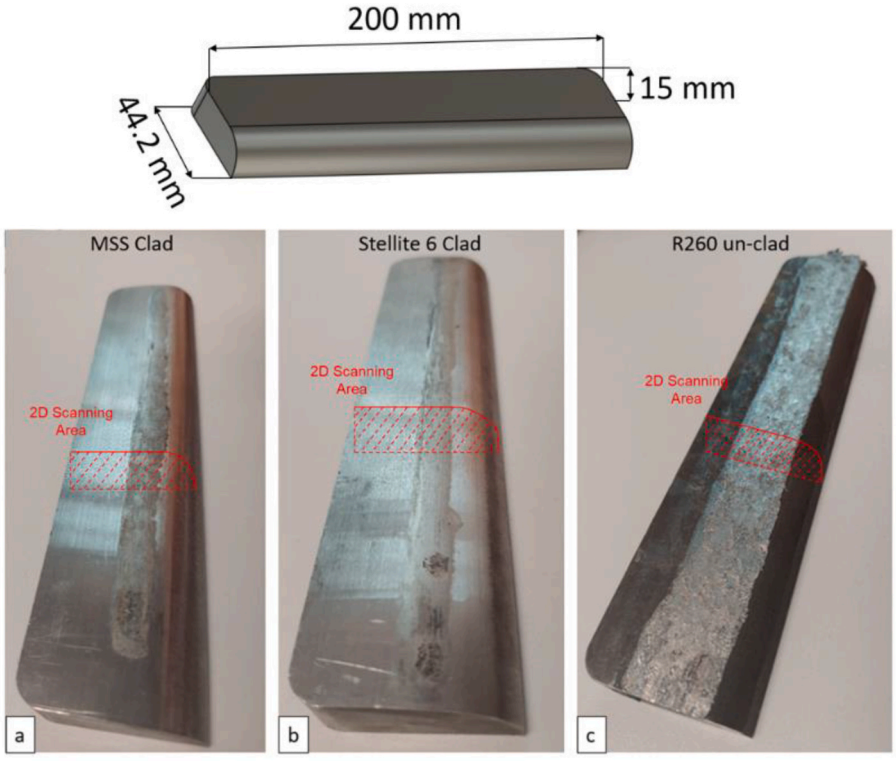

Fig. 4. Full scale test pockets after tests: a) MSS Clad pocket specimen b) Stellite 6 pocket specimen c) R260 un-clad pocket specimen.

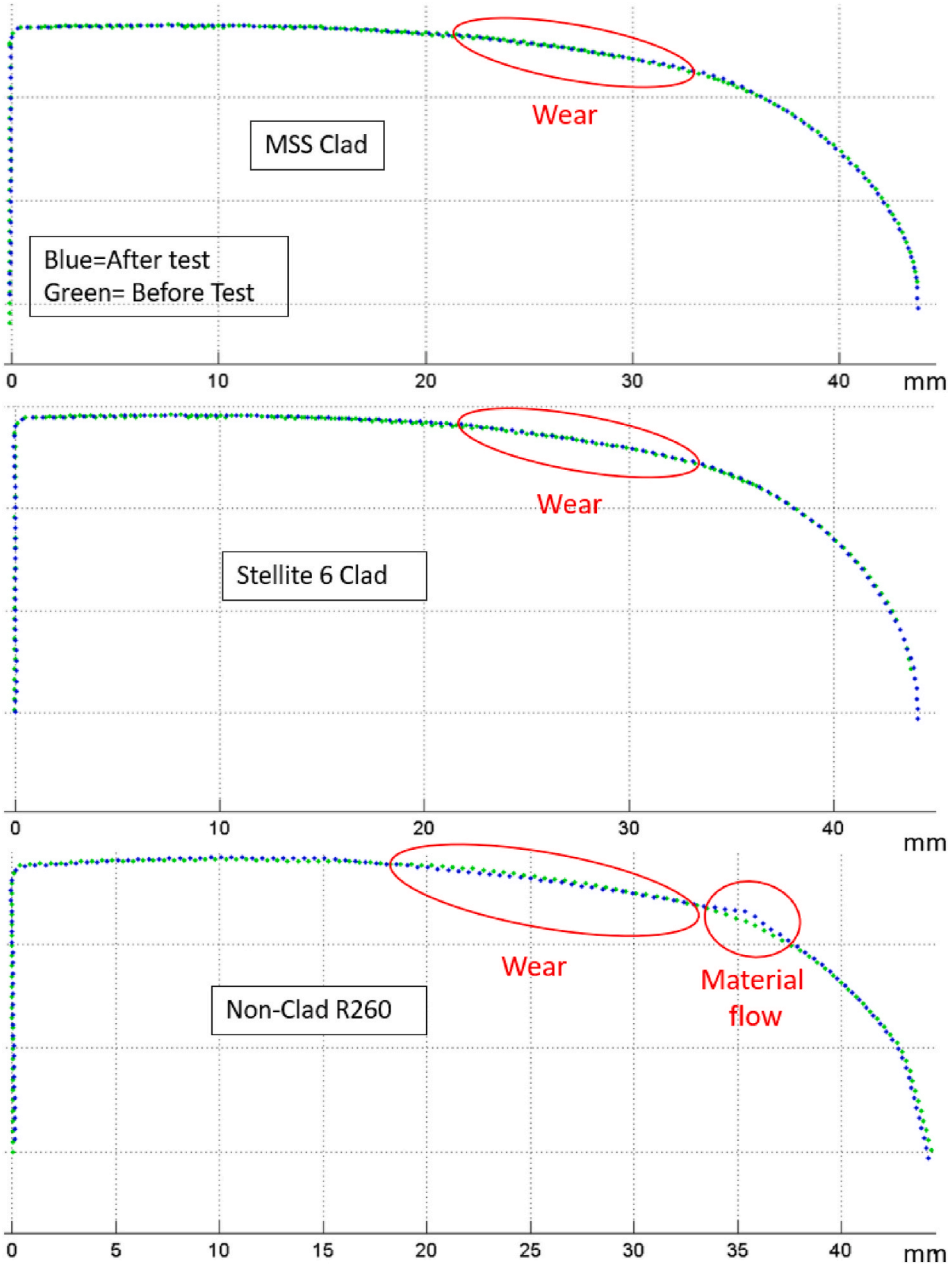

Fig. 5. Full Scale tests pocket specimen profiles before and after the tests by using Calipri profile measurement tool.

comparison and is shown with a white line. R260 is shown as a colour gradient line and the main difference can be seen with the dark blue colour and it is almost −0.4 mm lower than the MSS clad profile due its higher wear. The Stellite 6 and R260 pocket 2D profile comparison can be seen in the lower part of Fig. 6. Here the R260 pocket specimen was chosen as the reference profile and is shown as a white line. The Stellite 6 clad pocket profile can be seen as a line with a colour gradient. It shows that the R260 pocket specimen profile is around 0.200 mm lower than Stellite 6 profile in the contact area. Also, plastic deformation can be seen easily on the edge where the white line of the R260 rises above that of the Stellite 6. The comparisons clearly show that the un-clad R260 has the highest deformation and wear.

Images of the specimen surfaces are presented in Fig. 7. The MSS and Stellite 6 clad layer and un-clad R260 surface images show how the pockets deformed/wore and how wear tracks formed during after the 5000 full-scale cycles. The red lines with dimensions show the extent of the wear band after the tests. It can be seen that the un-clad R260 was damaged more, and the contact patch exhibits far more severe wear than the other clad pocket specimens. Flaking and local deformation is visible. As in the other measurements, the MSS and Stellite 6 pockets show similar contact zones after the completed cycles. The surfaces have an almost polished look to them, but there is some evidence of mild abrasive scratching.

The lateral and longitudinal measurements of roughness can be seen in Fig. 8. The commonly used roughness parameter, Ra, was used for these measurements. The clad layer roughness reduced following running backing up the observation of "polishing'' in the wear scars. Unsurprisingly the unclad R260 roughness increased. The effect of rail roughness on harder materials in determining near surface stress driving plasticity and wear is the subject of recent investigation [17]. The results here show clad materials are not only harder than conventional steel but also run to a smoother surface, thereby reducing routes to damage in two ways simultaneously.

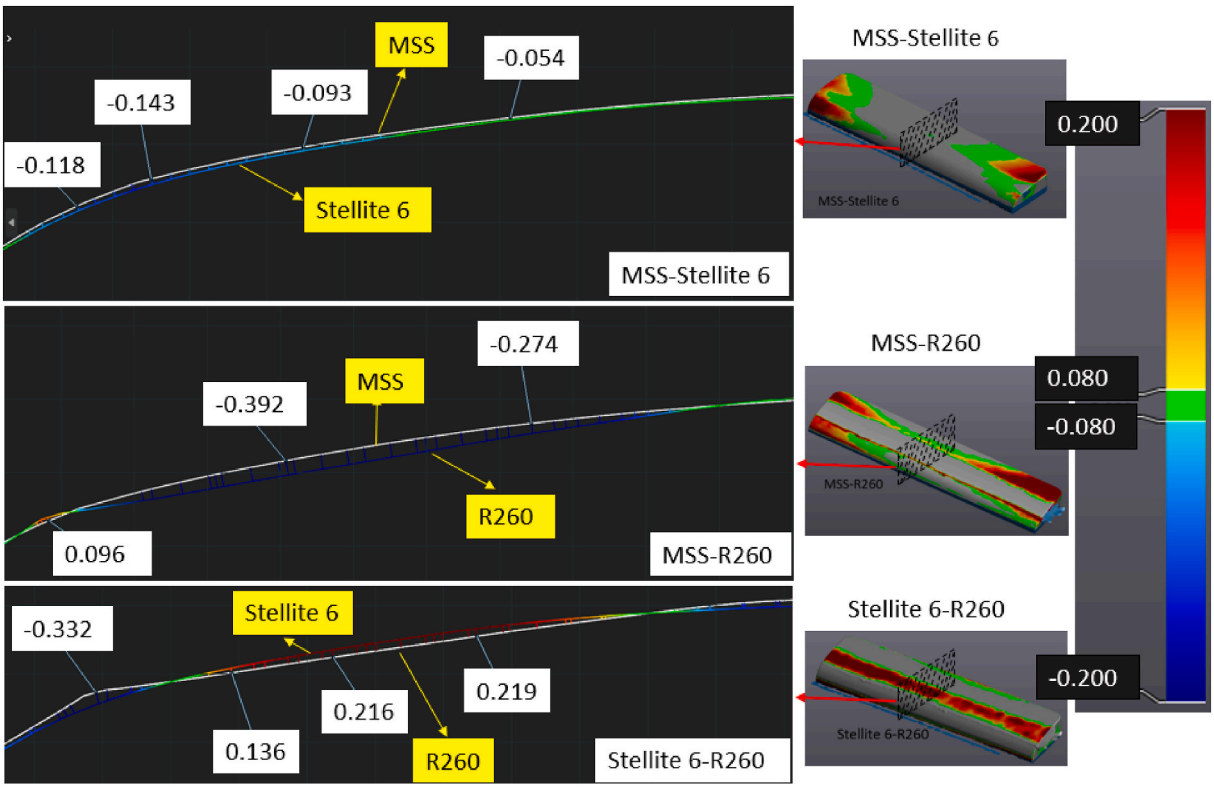

Fig. 6. Full-scale test pocket specimen scans after the tests using a Creaform 3D Laser Scanner.

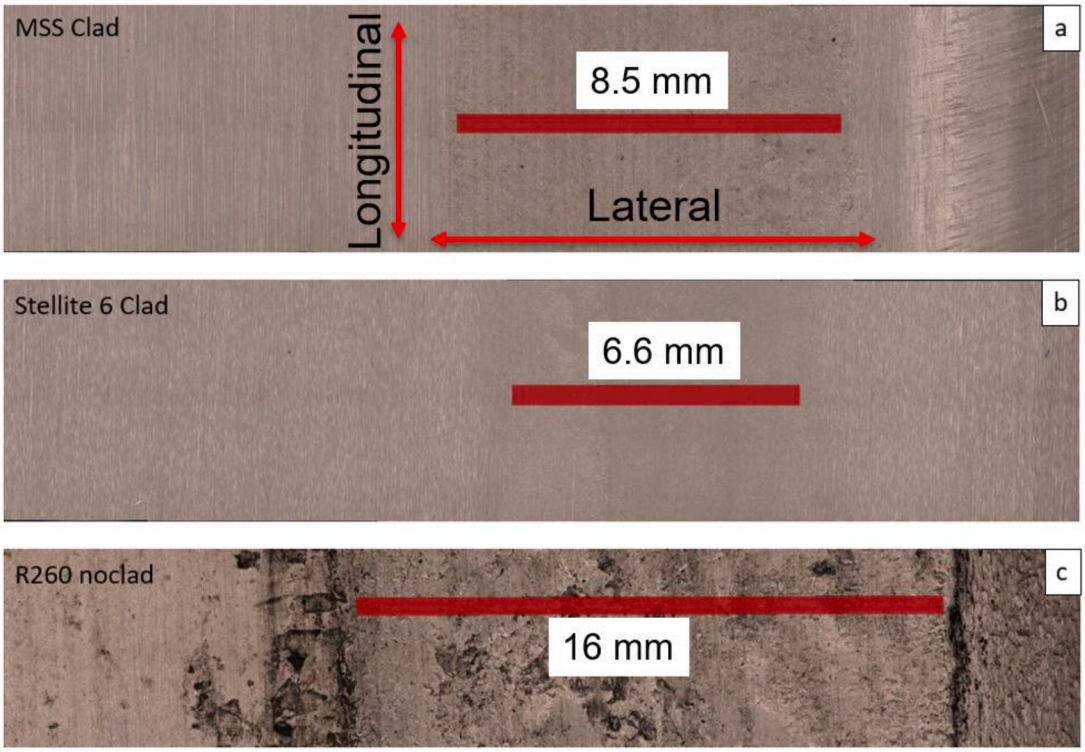

Fig. 7. Surface images of the pocket specimens after 5000 cycles taken using an Alicona non-contact profilometer.

3.2. Sub-surface analysis

After the full-scale rolling/sliding tests on the pocket samples were completed and all other measurements and images taken, they were sectioned and prepared for microstructural analysis. After mounting, grinding, and polishing the samples were etched to expose the microstructural features.

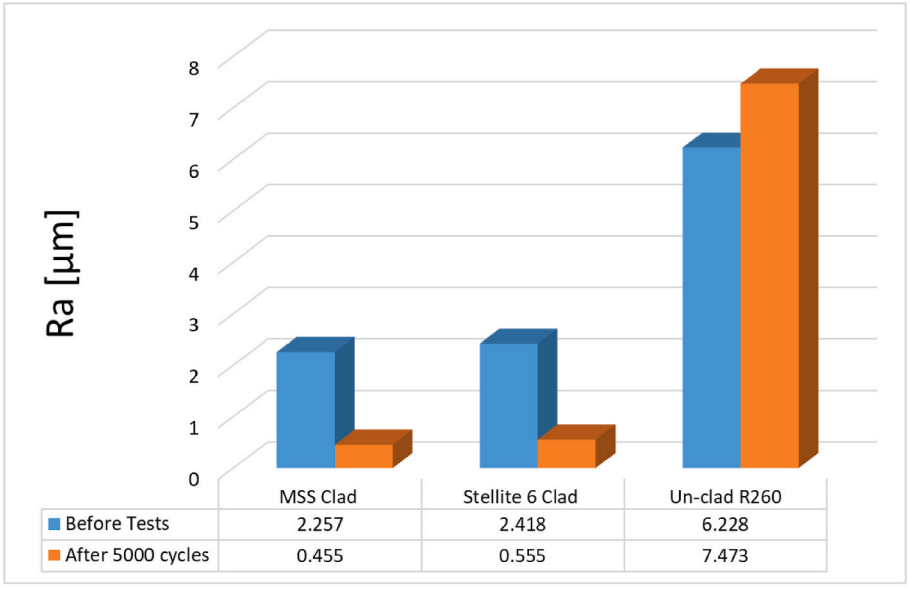

a)

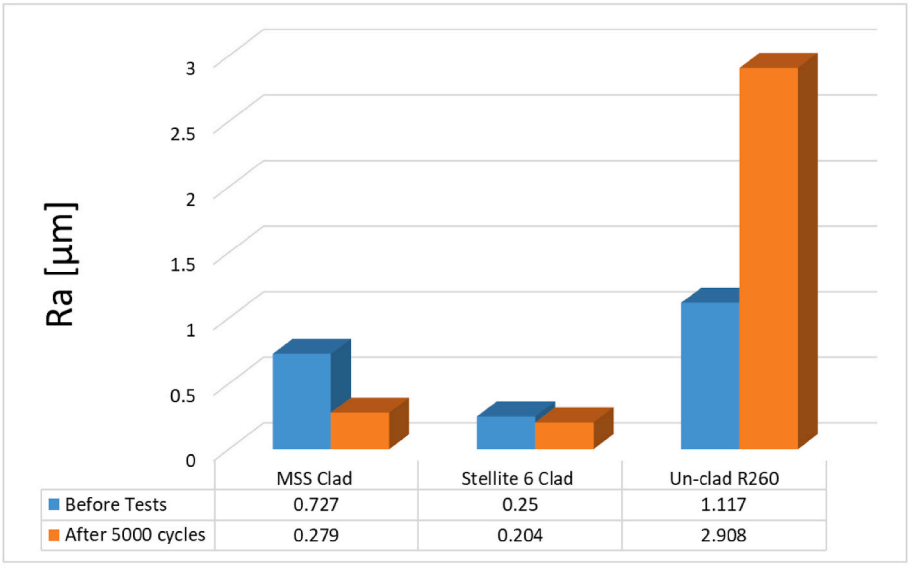

b)

Fig. 8. Pocket specimen roughness values before and after the 5000 cycle tests: a) lateral b) longitudinal.

3.2.1. *MSS clad*

Fig. 9 shows the sectioned MSS clad specimen. Two different microstructures are visible in the clad layer. Clearly the thermal processing has led to a different structure in the initial layer to the top layer. In the HAZ there is also a varying microstructure. This was seen in twin-disc testing as well [10]. Some light deformation and flake formation is visible. Again, this is similar to that seen in twin-disc testing [10] and indicates some ratchetting strain accumulation is occurring.

Fig. 10 shows the MSS clad and R260 substrate zone bonding. The images show a good bond between two materials in the transition (HAZ) zone. The diffusion zone can be seen clearly on the images as well.

In Fig. 11 on the surface of the Stellite 6 clad it can be seen there is no visible deformation after the 5000 cycles. The microstructure of the Stellite 6 coating shows both inter-dentritic and dentrite structures. The inter-dentritic structure is the darker colour of the structure in the clad part and the dentritic structure is brighter colour. There is no visible subsurface deformation. The SEM images show a small amount of spalling over surface (see Fig. 11(d)).

Fig. 12 shows the Stellite 6 clad and R260 substrate zone bonding. Again, a good bond is shown, and the diffusion zone is clear. SEM images shows the microstructure changes clearly from clad part to HAZ part (see Fig. 12(d–e)).

Fig. 13 shows the un-clad R260 pocket sample after etching. There is more deformation on the R260 pocket sample than the two clad pocket samples. The optical microscopy images show extensive plastic deformation. There are significant flakes visible on the surface. Crack growth can be seen from surface to the bulk material as well.

3.3. *Hardness*

Fig. 14 shows the hardness of the full-scale pockets after tests. It shows both nano-hardness and micro-hardness data. Nano-hardness data shows higher values than micro-hardness. Nano-hardness measurements were carried out as they could be achieved closer to the

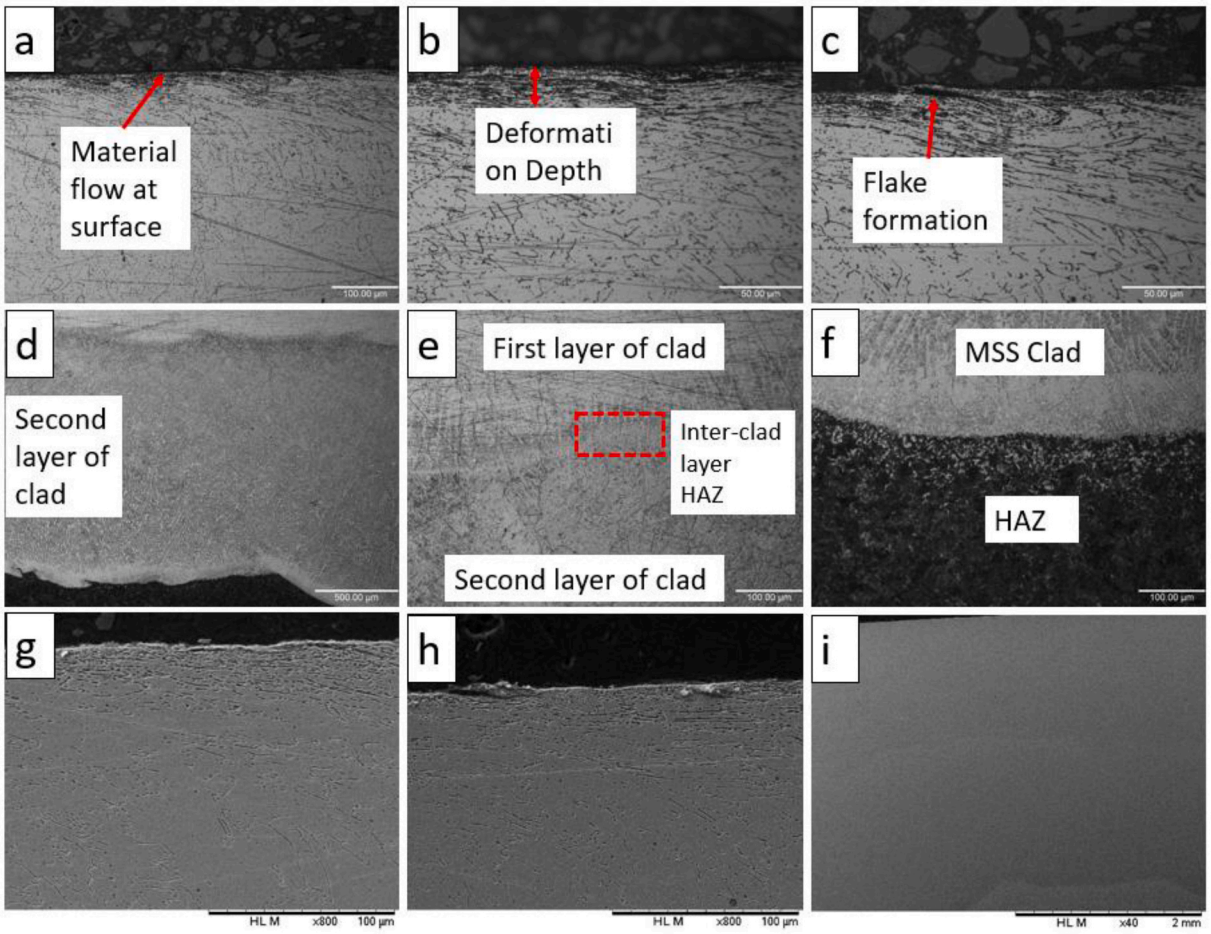

Fig. 9. MSS Clad pocket test sub-surface microstructure images from optical microscopy (a–f) and SEM (g–i).

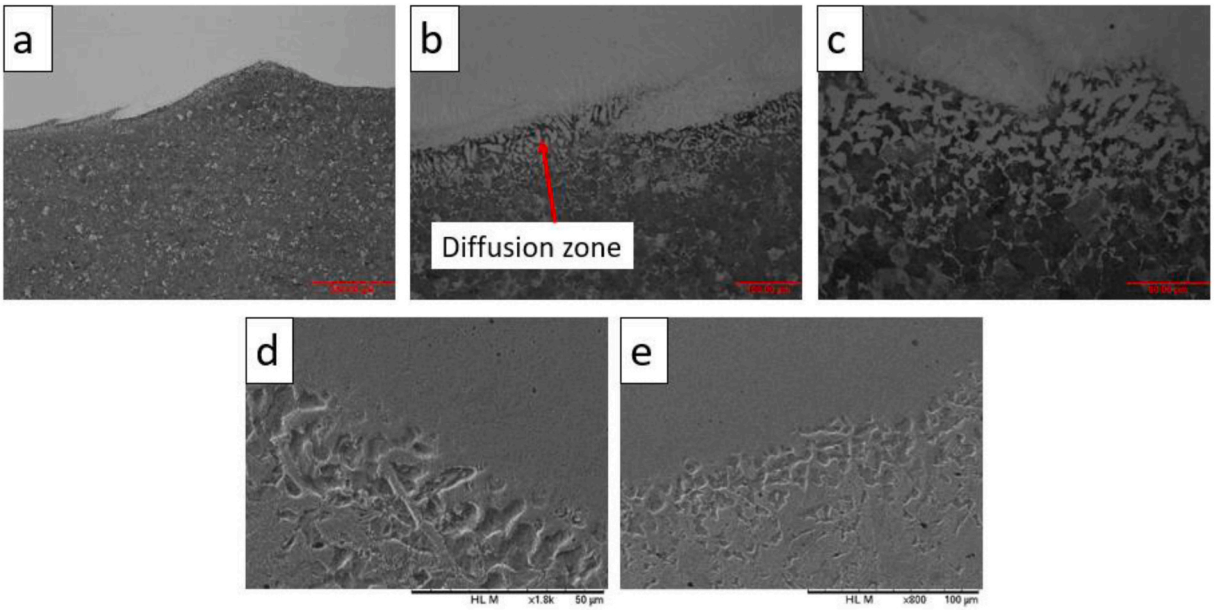

Fig. 10. MSS Clad pocket test clad and substrate part bonding microstructure images from optical microscopy (a–c) and SEM (d–e).

specimen contact surfaces. The surface hardness is 1046 HV on the MSS, 1228 HV on the Stellite 6 and 830 HV in the R260. Nano-hardness values show big differences from micro-hardness values because care must be taken with interpreting the data as typically values from nano-indentation are higher than the micro-hardness values by about 30 % [25]. The main reason for this is that nano-indentations use the

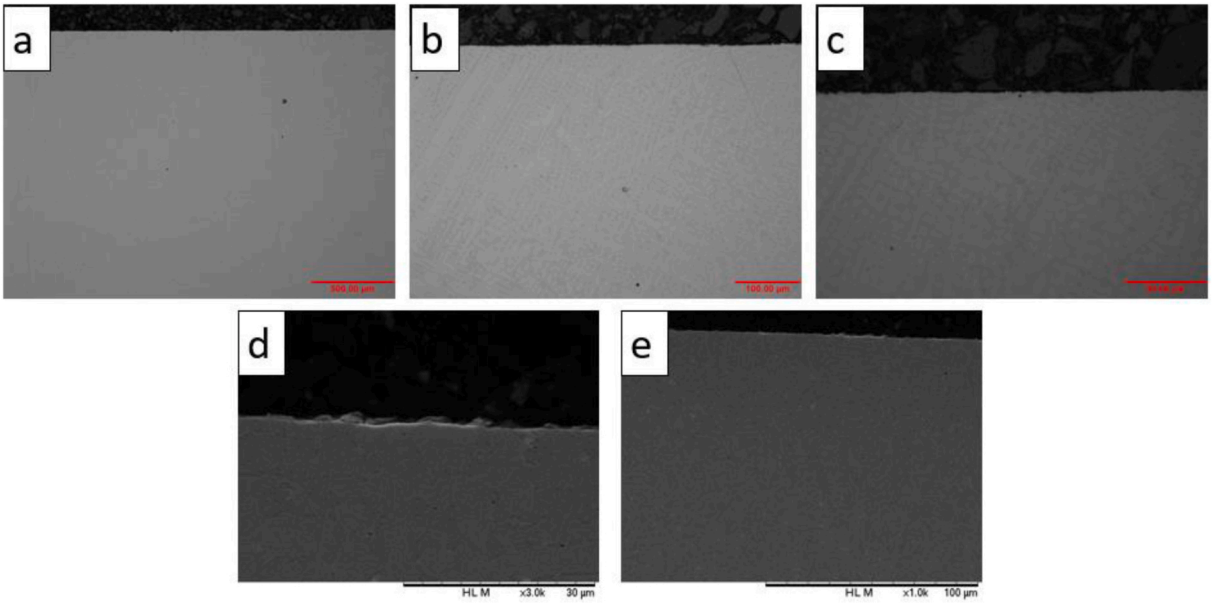

Fig. 11. Stellite 6 Clad pocket test sub-surface microstructure images from optical microscopy (a–c) and SEM (d–e).

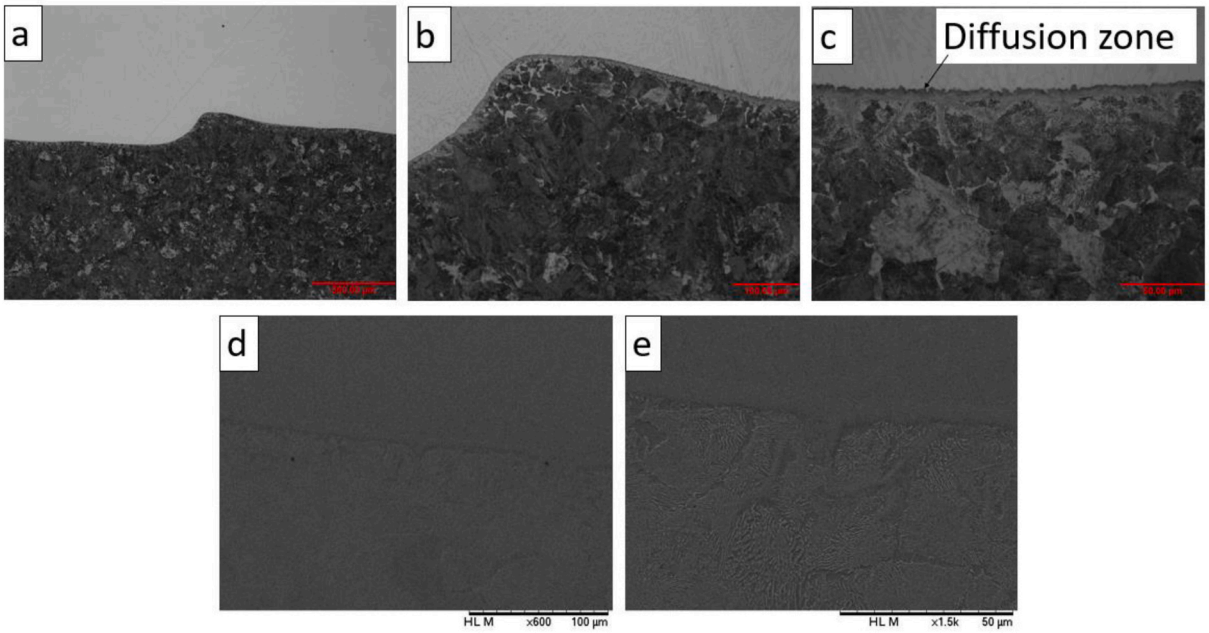

Fig. 12. Stellite 6 Clad pocket tests clad and substrate part bonding microstructure images from microscope and SEM.

projected contact area at peak load, however, micro-hardness uses residual projected area.

The micro-hardness data covers the clad layer through to the bulk material. The unclad R260 pocket as expected had the lowest hardness data. However, it had work hardened considerably as is show from the hardness difference between the surface and the bulk. The Stellite 6 clad layer has slightly higher hardness than MSS clad layer. In the substrate part for both clad layers the hardness was similar.

4. Discussion

4.1. Wear mechanisms

The un-clad R260 shows evidence of higher wear and deformation than the clad layers through all the measurements. The surface flakes (which caused the surface roughness to increase) and the sub-surface deformation indicate that a ratchetting mechanism dominates as has been seen in many other studies of rail material wear.

The clad layers experienced much less wear. The surfaces also became smoother during the tests. There was some indication of deformation in the sub-surface images, but this was an order of magnitude lower than that seen on the un-clad R260 (see Fig. 15). This matches observations from twin disc testing (see Figs. 15 and 16). In both twin-disc and full-scale testing the deformation was higher in the MSS than Stellite 6 which was probably due to the higher hardness of the Stellite 6 (see Fig. 14). The evidence suggests that ratchetting is not the dominant wear mechanism in the case of the clad layers and perhaps that mild abrasion was occurring which would explain the polishing effect that led to the lower post-test roughness. The lowering of roughness was also seen in twin disc testing of these materials (see Table 2)

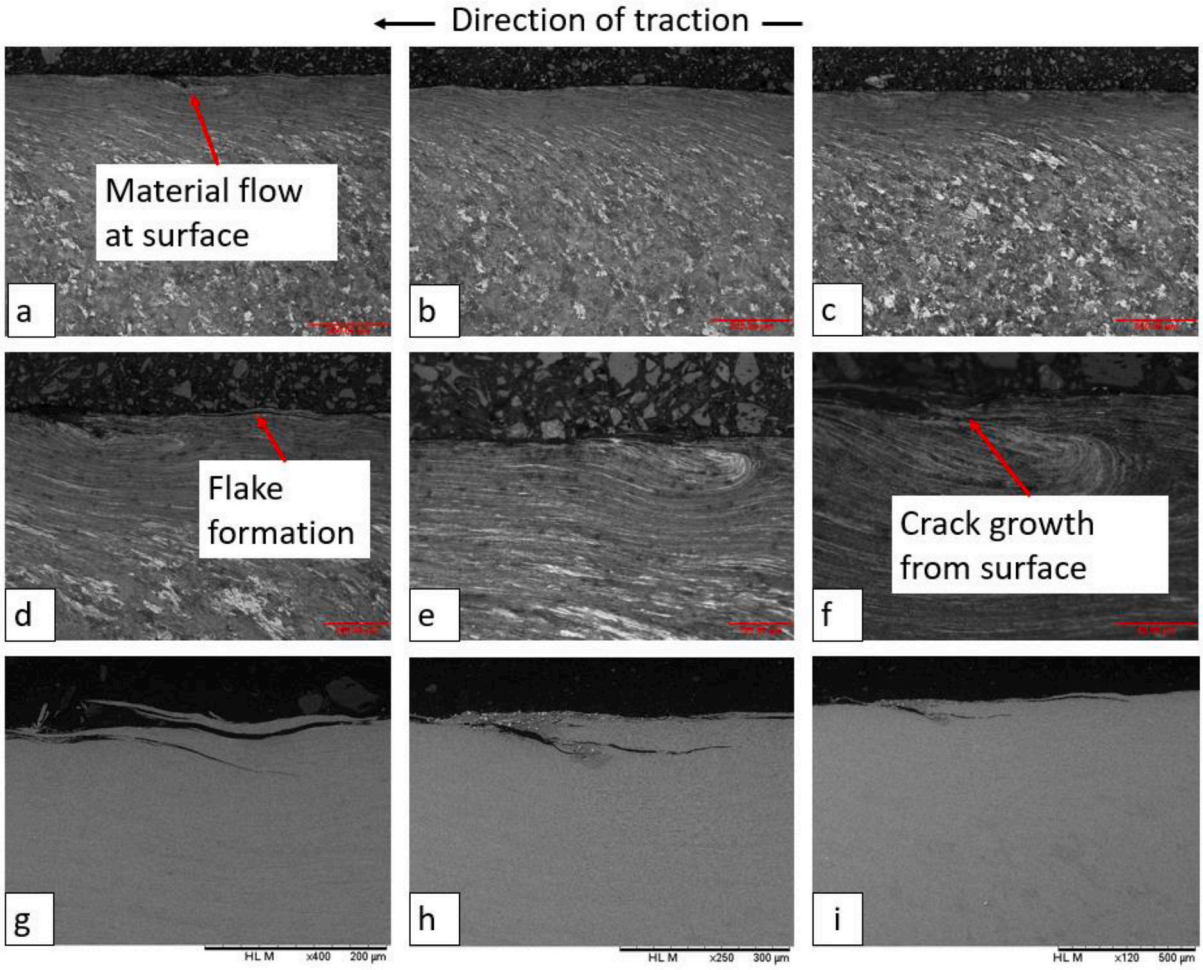

Fig. 13. R260 un-clad pocket test microstructure images from optical microscopy (a–f) and SEM (g–i).

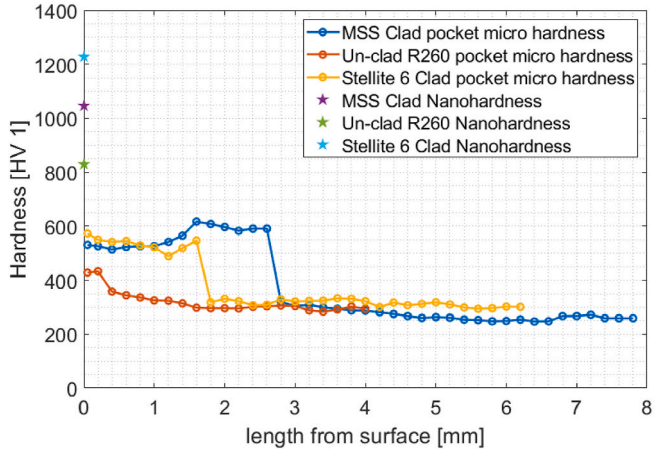

Fig. 14. Pocket full scale tests micro-hardness and nano-hardness after tests.

(while unpublished, the data is for tests carried out in Ref. [9]).

4.2. Wear rates

One approach that can be used to compare wear for different test scales is the $T\Upsilon$ method. $T\Upsilon$ (where T is the tractive force (friction coefficient × normal force) and Υ is the slip in the contact) is an indication of energy dissipated in the interface. This can be normalised by dividing by nominal contact area (A) allowing different contacts to be compared. It has been shown in the mild wear regime, that wear rate is proportional to $T\Upsilon/A$ [26]. Fig. 17 shows twin disc wear data for un-clad R260 and MSS and Stellite 6 clad layers from previous studies [10,4,26] along with the full-scale wear data from these tests. It can be seen that the wear rates fit the same linear relationship against $T\Upsilon/A$ Indicating that the full-scale results are in line with the twin-disc results. This shows it is valid to use twin-disc testing wear rates as a means to predict full scale wear through the $T\Upsilon$ method. The full-scale results also confirm that the clad layers perform well.

4.3. Hardness evolution

Final hardness values for the MSS clad and Stellite 6 compare well with those from twin disc testing as shown in Figs. 18 and 19 and Table 3. In Fig. 18, premium rails were listed with nae of R350, A, B, and C.

Work hardening trends between the small and full scale specimens are similar (as shown in Table 3). This is quite promising as the thermal processing between the two is different due to the size difference between the two and some hardness values may not be accurately comparable as they will have been taken at different depths.

4.4. Microstructure observations

Some interesting features were seen in the microstructure images of the clad layers that will be discussed here.

In Fig. 9(a-c,g,h), the MSS clad shows two phases with dendritic

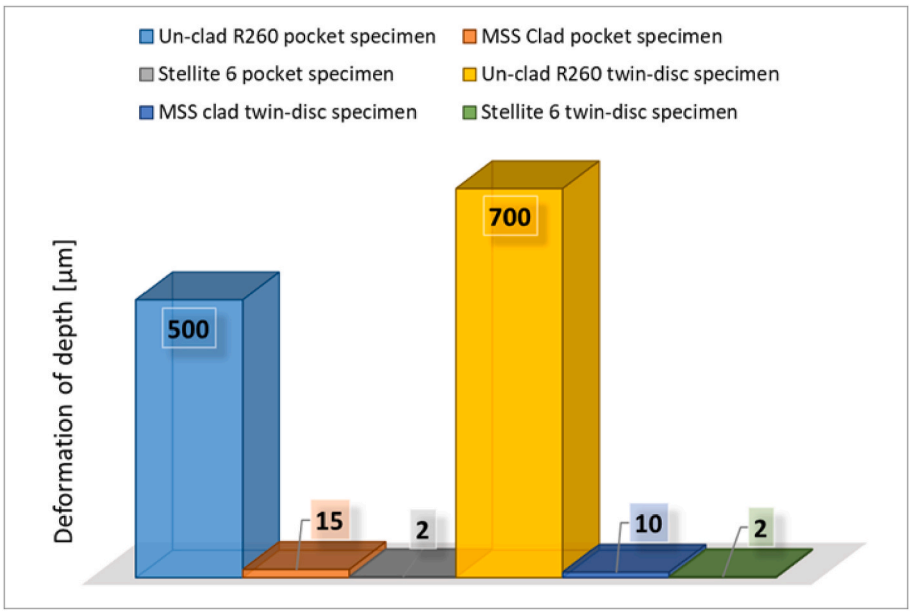

Fig. 15. Deformation of depths after the experiments from twin-disc tests by Ref. [10] and full-scale tests comparison.

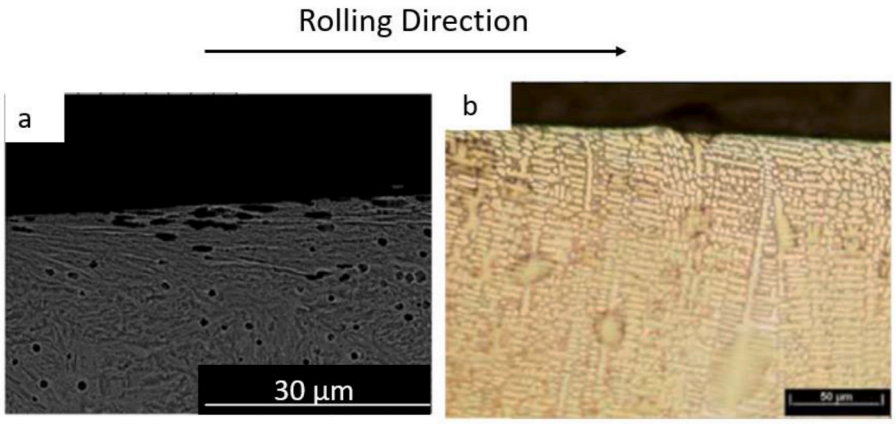

Fig. 16. Microstructures images after tests a) MSS clad twin disc sample after 30,000 cycles [10]; b) Stellite 6 clad twin-disc sample after 30,000 cycles [9].

solidification morphology, the black phase is clearly visible together with the white phase due to etching. The second phase may correspond to retained delta ferrite due to an incomplete peritectic transformation or a $M_{23}C_6$ carbide or both according to the pseudo-binary phase diagram in Fig. 20. The matrix has deformed on the surface and aligned these black phases to the runout of the deformation.

Fig. 9(e) shows a fascinating phenomenon. A heat-affected zone (HAZ) is formed within the melt zone of the first MSS clad pass. Thus, an aligned dendritic morphology is present in the region with higher heat input at the interface of the first and second pass, which austenitizes and returns to room temperature in a way that has less of a rough casting texture with a finer microstructure mainly on the recrystallization region. The regions with lower heat input may undergo recrystallization and recovery but tend to change morphology less. This phenomenon is known as "temper bead" [28]. For steels, that have a greater tendency to form untampered martensite during the weld, this temper bead helps to increase the toughness in these HAZ regions. However, tempered martensitic microstructures, even by temper bead, will soften locally in this region.

Fig. 10(b) reveals some important information. In the region described as the diffusion zone, phases similar to the pro-eutectoid morphology can be seen. To analyse this microstructure, the phase diagram in Fig. 20 is useful. Assuming that most of the substitutional alloying elements cannot get enough mobility and the fact the carbon, an interstitial alloying element, level in the MSS is considerably smaller than the rail (see Table 1), the carbon will be the one to migrate by diffusion toward the molten metal, generating this diffusion zone [29]. As shown in Fig. 20, when increasing the amount of carbon at high temperature, there may be a tendency to enter the liquid, delta ferrite (BCC), or austenite (FCC) at higher temperature and the precipitate in the form of carbide $M_{23}C_6$ region.

The Stellite 6 clad layer microstructure in Figs. 11(b and c) clearly shows the dendritic morphology of the molten zone, including the main direction tending towards heat extraction (pointing towards the surface). The dendritic morphology occurs due to the heat extraction/micro-segregation and is very characteristic of the molten zone.

In Figs. 12(b and e) it can be seen that at the rail adjacent to the clad metal, the microstructure presents pro-eutectoid ferrite decorating the former austenite grain boundaries with pearlite inside the grains. Diffusion leads to a local decrease of carbon concentration at the interface and tends to form pro-eutectoid ferrite. Pro-eutectoid ferrite found in rail welding also follows the prior austenitic grain boundary [30]. The same feature is observed in Fig. 10. The diffusion region causes the rail carbon (with higher concentration) to diffuse toward the molten

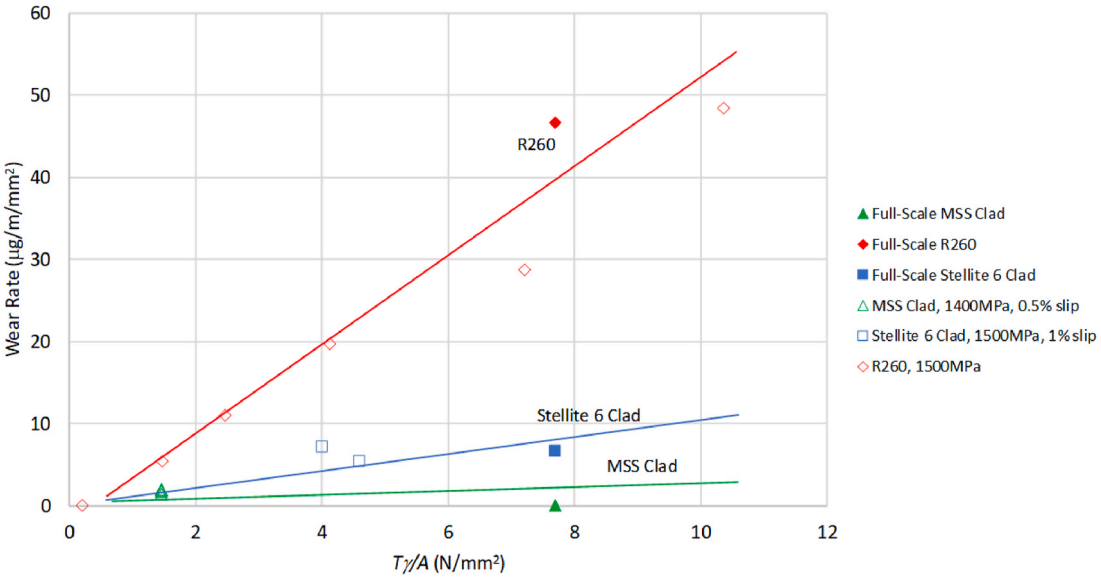

Fig. 17. Wear rates of full-scale rail pocket specimens and twin-disc specimens against $T\gamma/A$ approach.

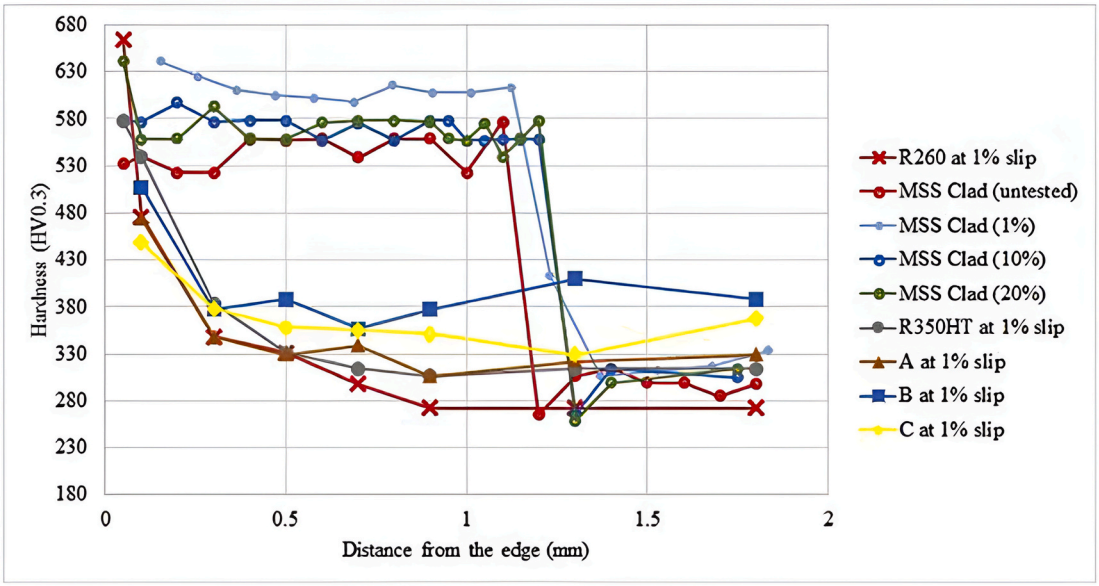

Fig. 18. Hardness data for a range of clad and un-clad materials after twin disc testing [7].

metal (MSS – lower concentration) and deplete it locally. The lower amount of carbon leads the rail to have a composition less than that of the eutectoid (see Table 1) and consequently forms pro-eutectoid ferrite on cooling.

Throughout the images where the HAZ below the clad layer is visible an evolution is visible as the depth increases towards the bulk R260 microstructure (for example Fig. 9(f)). This was also described in detail in twin-disc testing of MSS clad layers [10]. It follows the observations made by, amongst others, Mansouri and Monshi [27] and is similar to that seen in rail welds.

Figs. 9, 12, 13 and 16 depict the microstructure in the cross-section after the wear test region. Figs. 9 and 16, illustrating the surface of MSS steel clad, clearly show plastic deformation on the surface resulting in flake formation. This plastic deformation is prominently visible by tracking and aligning the microstructure towards the friction of the test. Conversely, Fig. 11, displaying the surface of Stellite 6 clad, does not exhibit any signs of deformation. However, due to Stellite 6's considerably higher hardness compared to the bulk microstructure (pearlitic rail, indications of subsurface deformation can be observed at the clad bonding region, as indicated in Fig. 12. Nevertheless, Fig. 16(b) demonstrates a shallow surface deformation on the Stellite 6 clad due to its significantly greater hardness. A more detailed comparison of surface deformation between these two clads can be better observed in Fig. 16.

The microstructure after the R260 steel test without clad reveals a much greater depth of plastic deformation compared to the MSS clad, exhibiting a more pronounced alignment of the microstructure. In addition to flake formation, the test also showed the formation of RCF cracks due to both superficial and subsurface plastic deformation.

5. Conclusions

Full-scale tests have been carried out of clad rail samples and an un-clad R260 reference sample. All samples were analysed using a range of measurements to allow a comparison between the clad and un-clad rail

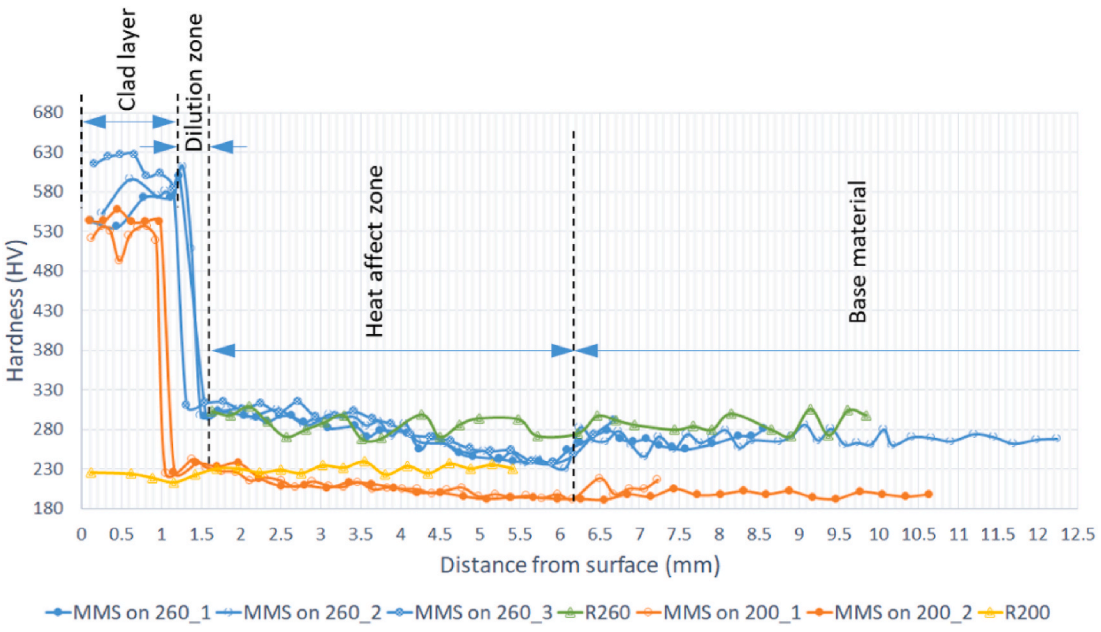

Fig. 19. Hardness data for clad layers from previous twin disc testing [10].

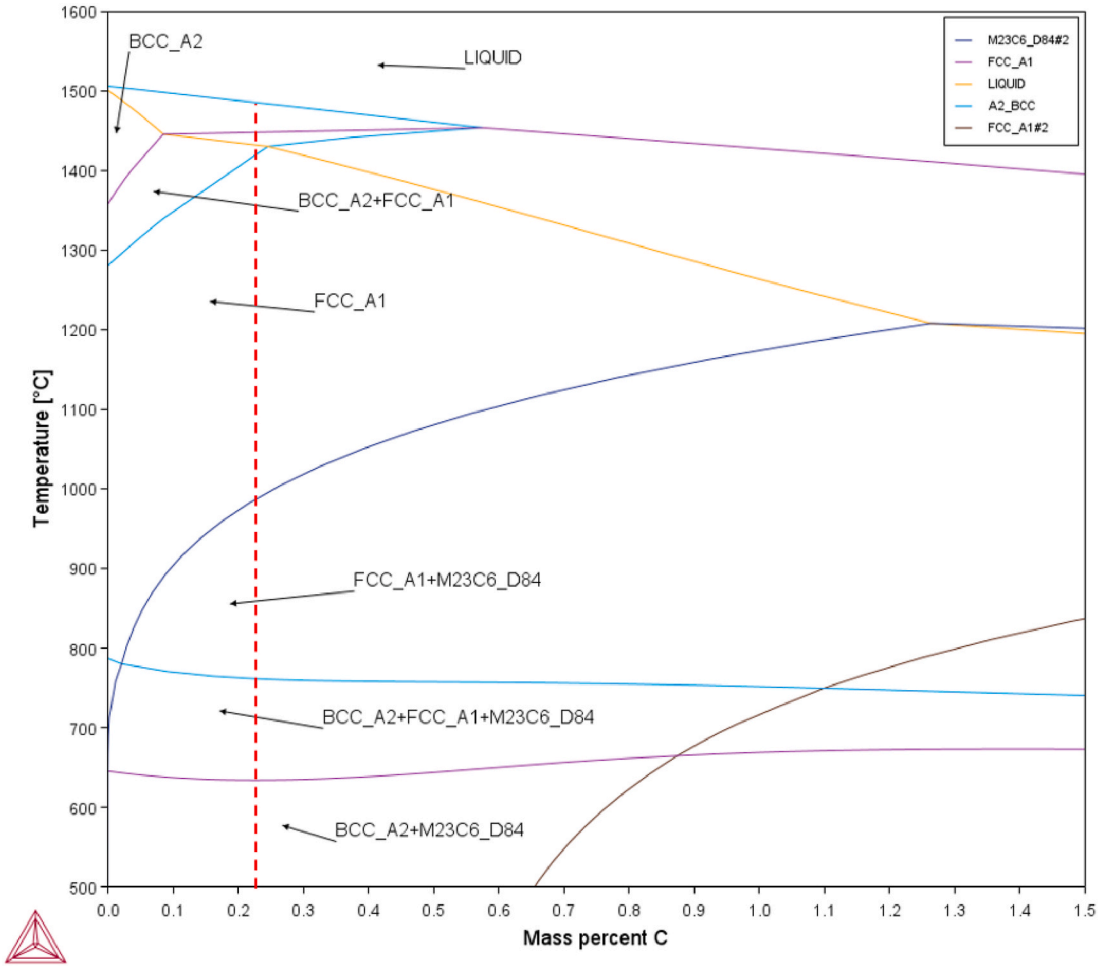

Fig. 20. Pseudo-binary diagram of steel with similar chemical composition to MSS clad deposited layer calculated by Thermocalc® software.

Table 1
Chemical compositions (%by mass) of R260, MSS, Stellite 6, and E8 wheel materials [21–24].

	C	Mn	Si	Cr	Ni	Mo	Co	V	W	N	Al	S	P
R260	0.74	1.08	0.31	0.040	–	–	–	0.004	–	–	0.003	0.018	0.013
MSS	0.06	1.22	0.46	14.64	3.31	0.42	2.01	0.51	0.62	0.04	0.01	0.005	0.009
St. 6	1.0	<0.1	0.9	27.0	–	–	Bal	–	4	–	–	–	–
E8	0.542	0.734	0.253	0.141	0.120	0.048	–	0.006	–	–	–	0.006	0.011

Table 2
Comparison of roughness Ra [μm] between test scales and materials.

Reference	Test	Material	Initial Roughness (Ra [μm])	Final Roughness (Ra [μm])	Percentage Roughness Change (((final/initial roughness) × 100)-100)
Lewis et al. (2016)	Twin disc	MSS	1.66	1.09	−33 %
Lewis et al. (2016)	Twin disc	Stellite 6	1.70	1.00	−41 %
Lewis et al. (2016)	Twin disc	R260	0.84	5.16	514 %
Current study	Full-scale	MSS	2.257	0.455	−80 %
Current study	Full-scale	Stellite 6	2.418	0.555	−77 %
Current study	Full-scale	R260	6.228	7.473	20 %

Table 3
Comparison of clad layer micro-hardness between current full-scale tests and previous twin disc testing.

Reference	Test	Material	Initial Hardness [Hv]	Final Hardness [Hv]	Percentage Work Hardening (((final/initial hardness) × 100)-100)
Lu et al. [10]	Twin disc	MSS	–	630	–
Christoforou et al. [7]	Twin disc	MSS	–	640	–
Lewis et al. [9]	Twin disc	MSS	607	805	+33 %
Lewis et al. [9]	Twin disc	Stellite 6	647	786	+22 %
Lewis et al. [9]	Twin disc	R260	308	784	+154 %
Current study	Full-scale	MSS	600	804[a]	+34 %
Current study	Full-scale	Stellite 6	550	944[a]	+71 %
Current study	Full-scale	R260	300	638[a]	+113 %

[a] Micro-hardness value estimated by dividing nano-hardness value by 1.3 (based on [25]).

behaviour as well as comparisons with previous twin disc testing of the same materials.

The MSS and Stellite 6 clad layers performed very well in the tests exhibiting far less wear, plastic flow and crack formation than the unclad R260 material. This confirms what was seen in previous twin disc testing. The clad materials stayed well bonded and are clearly a good solution for assessment in field trials.

The good correlation between the twin-disc testing and full-scale testing across wear rates, mechanisms, work hardening, and roughness evolution shows that the outcomes of small-scale tests are good indicators of full-scale behaviour for reducing the amount of full-scale testing needed in assessing future potential clad materials.

The observations of the microstructures, particularly around the differences seen in different layers when multiple layers were applied will be very useful in designing approaches for cladding in the future to create specific microstructures in the clad layers.

Author contribution

Kazim Yildirimli: Supervisor; Conceptualisation; Project Administration; Investigation. Methodology; Writing – review and editing. Roger Lewis: Supervisor; Conceptualisation; Project Administration; Investigation; Methodology; Writing – review and editing. David Fletcher: Investigation; Methodology. Zing S. Lee: Investigation; Methodology. Henrique Boschetti Pereira: Methodology, Writing. Helio Goldenstein: Methodology, Writing.

The authors confirm that this is original work, and the paper has not been submitted elsewhere for publication.

Declaration of competing interest

The authors declare the following financial interests/personal relationships which may be considered as potential competing interests: Kazim Yildirimli reports financial support was provided by The Turkish Ministry of National Education. Roger Lewis reports financial support was provided by Engineering and Physical Sciences Research Council.

Data availability

Data will be made available on request.

Acknowledgements

Kazim Yildirimli was supported by the Turkish Ministry of National Education by providing a scholarship.

The work was part funded by the EPSRC project “Alchemy” (EP/M023044/1).

References

[1] S.R. Lewis, R. Lewis, P.S. Goodwin, S. Fretwell-Smith, D.I. Fletcher, K. Murray, J. Jaiswal, Full-scale testing of laser clad railway track; case study – testing for wear, bend fatigue and insulated block joint lipping integrity, Wear 376 (377) (2017) 1930–1937.

[2] F.J. Franklin, G.J. Weeda, A. Kapoor, E.J.M. Hiensch, Rolling contact fatigue and wear behaviour of the Infrastar two-material rail, Wear 258 (7–8) (2005) 1048–1054.

[3] A. Clare, O. Oyelola, J. Folkes, P. Farayibi, Laser cladding for railway repair and preventative maintenance, J. Laser Appl. 24 (3) (2012) 032004.

[4] S.R. Lewis, R. Lewis, D.I. Fletcher, Assessment of laser cladding as an option for repairing/enhancing rails, Wear 330 (331) (2015) 581–591.

[5] A. Narayanan, M. Mostafavi, T. Pirling, S. Kabra, R. Lewis, M.J. Pavier, M.J. Peel, Residual stress in laser cladded rail, Tribol. Int. 140 (2019) 105844.

[6] S. Niederhauser, B. Karlsson, Fatigue behaviour of Co-Cr laser cladded steel plates for railway applications, Wear 258 (7–8) (2005) 1156–1164, https://doi.org/10.1016/j.wear.2004.03.026.

[7] P. Christoforou, D.I. Fletcher, R. Lewis, Benchmarking of premium rail material wear, Wear (2019) 436–437, https://doi.org/10.1016/j.wear.2019.202990.
[8] X. Wang, L. Lei, H. Yu, A review on microstructural features and mechanical properties of wheels/rails cladded by laser cladding, Micromachines 12 (2) (2021) 1–16, https://doi.org/10.3390/mi12020152.
[9] S.R. Lewis, et al., Improving rail wear and RCF performance using laser cladding, Wear 366 (367) (2016) 268–278.
[10] P. Lu, S.R. Lewis, S. Fretwell-Smith, D. Engelberg, D.I. Fletcher, R. Lewis, Laser cladding of rail; the effects of depositing material on lower rail grades, Wear 438–439 (2019) 203045, https://doi.org/10.1016/j.wear.2019.203045.
[11] K. Yildirimli, K. Tomlinson, D.I. Fletcher, R. Lewis, Small-scale testing of rail laser cladding longevity, parameter tolerance and in-situ repairs in preparation for field implementation, in: Proceedings of CM2022, 12th International Conference on Contact Mechanics and Wear of Rail/Wheel Systems, Melbourne, Australia, September 2022, pp. 4–8.
[12] Y. Zhu, Y. Yang, X. Mu, W. Wang, Z. Yao, H. Yang, Study on wear and RCF performance of repaired damage railway wheels: assessing laser cladding to repair local defects on wheels, Wear 430–431 (2019) 126–136.
[13] K. Tomlinson, D.I. Fletcher, R. Lewis, Evaluation of laser cladding as an in-situ repair method on rail steel, Tribol. Int. 180 (2023) 108210.
[14] W.J. Wang, Z.K. Fu, X. Cao, J. Guo, Q.Y. Liu, M.H. Zhu, The role of lanthanum oxide on wear and contact fatigue damage resistance of laser cladding Fe-based alloy coating under oil lubrication condition, Tribol. Int. 94 (2016) 470–478, https://doi.org/10.1016/j.triboint.2015.10.017.
[15] T. Xie, et al., Investigation on the rolling contact fatigue behaviors of different laser cladding materials on the damaged rail, J. Tribol. 143 (2021) 51108–51109, https://doi.org/10.1115/1.4050690.
[16] In2Track INT-T2.2-NRI-001-02, 2016.
[17] K. Tomlinson, D.I. Fletcher, R. Lewis, Measuring material plastic response to cyclic loading in modern rail steels from a minimal number of twin-disc tests, J. Rail Rapid Transit, Proc. IMechE, Part F 235 (2023) 1203–1213.
[18] F.C. Robles Hernández, A.O. Okonkwo, V. Kadekar, T. Metz, N. Badi, Laser cladding: the alternative for field thermite welds life extension, Mater. Des. 111 (2016) 165–173, https://doi.org/10.1016/j.matdes.2016.08.061.
[19] S. Fukagai, H.P. Brunskill, A.K. Hunter, R.S. Dwyer-Joyce, R. Lewis, Transitions in rolling-sliding wheel/rail contact condition during running-in, Tribol. Int. 149 (2020) 105679, https://doi.org/10.1016/j.triboint.2019.03.037.
[20] M. Harmon, J.F. Santa, J.A. Jaramillo, A. Toro, A. Beagles, R. Lewis, Evaluation of the coefficient of friction of rail in the field and laboratory using several devices, Tribol. Mater. Surface Interfac. 14 (2) (2020) 119–129, https://doi.org/10.1080/17515831.2020.1712111.
[21] "Stellite 6 Alloy Datasheet", https://www.deloro.com/fileadmin/users/redakteur/006_Downloads/Data_Sheets/Deloro_MDS_Stellite6_rev00.pdf, accessed 21/2/23.
[22] "Martensitic Stainless Steels Datasheet", https://bssa.org.uk/wpcontent/uploads/2021/02/Martensitics_JB_2.pdf, accessed 21/2/23.
[23] K. Aniołek, Abrasive wear of railway sections of steel with a different pearlite morphology in railroad switches, J. Achieve. Mater. Manufact. Eng. 43 (1) (2010) 236–243.
[24] J.F. Santa, P. Cuervo, P. Christoforou, M. Harmon, A. Beagles, A. Toro, R. Lewis, Twin disc assessment of wear regime transitions and rolling contact fatigue in R400HT – E8 pairs, Wear 432–433 (2019) 102916, https://doi.org/10.1016/j.wear.2019.05.031.
[25] L. Qian, M. Li, Z. Zhou, H. Yang, X. Shi, Comparison of nano-indentation hardness to microhardness, Surf. Coating. Technol. 195 (2–3) (2005) 264–271, https://doi.org/10.1016/j.surfcoat.2004.07.108.
[26] R. Lewis, R.S. Dwyer-Joyce, "Wear mechanisms and transitions in railway wheel steels," Proceedings of the IMechE, Part J J. Eng. Tribol. 218 (2004) 467–478.
[27] H. Mansouri, A. Monshi, Microstructure and residual stress variations in weld zone of flash-butt welded railroads, Sci. Technol. Weld. Join. (3) (2004) 237–245, vo. 9.
[28] P.R. Vishnu, Solid-state transformations in weldments: HAZ in multipass weldments, ASM Handbook 6 (1993).
[29] H. Bhadeshia, R. Honeycombe, Steels: Microstructure and Properties, third ed., Butterworth-Heinemann, 2006, pp. 8–13.
[30] L.P. Nishikawa, H. Goldenstein, Divorced eutectoid on heat-affected zone of welded pearlitic rails, J. Miner. Met. Mater. Soc. 71 (2) (2019) 815–823.
[31] T. Jendel, "Prediction of Wheel Profile Wear – Methodology and Verification", Licentiate Thesis, TRITA-FKT, vol. 9, Royal Institute of Technology, Stockholm, Sweden, 2000.